JOURNAL OF MATERIALS SCIENCE: MATERIALS IN ELECTRONICS **16** (2005) 703 – 713

REVIEW

Photoconductivity methods in materials research

MONICA BRINZA, JAN WILLEKENS, MOHAMMED L. BENKHEDIR, EVGUENIA V. EMELIANOVA, GUY J. ADRIAENSSENS
University of Leuven, Laboratorium voor Halfgeleiderfysica, Celestijnenlaan 200D, B-3001 Leuven, Belgium

Photoconductivity refers to the incremental change upon illumination of the electrical conductivity of a substance. For semiconductors and insulators, where the conductivity in the dark is low, significant changes can be measured. From the dependence of the photoconductivity on factors such as the exciting photon energy, the intensity of the illumination or the ambient temperature, significant information can be derived on the distribution of electronic states in the material and on carrier generation and recombination processes. Those results in turn provide indications about optical absorption coefficients or concentrations and distributions of defects in the materials. Both steady-state currents under constant illumination and transient methods involving pulsed excitation can be used to study the electronic density of states as well as the recombination. The transient time-of-flight technique further allows the determination of carrier drift mobilities. Photocurrents can also be used to measure interface barriers through internal photoemission or to detect electron spin resonance.
© 2005 Springer Science + Business Media, Inc.

1. Introduction

Photoconductivity has traditionally played a significant role in materials research, and most notably so in the study of covalently bonded semiconductors and insulators. Indeed, being the incremental conductivity generated by the absorption of (optical) photons, photoconductivity can be most clearly resolved in situations where the intrinsic dark conductivity of the material is low. This conductivity in the dark, leading to the so-called dark current, is due to the thermal equilibrium density of free carriers in the material and has to be subtracted from any measured current to obtain the actual photocurrent. The basic processes that govern the magnitude of the photocurrent are the generation of free electrons and holes through the absorption of incident photons, the transport of those free carriers through the material under the influence of an electric field, and the recombination of the photo-excited electrons and holes. The study of any of those aspects as a function of the characteristics of the current-inducing illumination, as well as the study of their time development upon changes in that illumination, will offer insights into the structure and electronic properties of the material under investigation. However, given the fact that three separate processes are involved in producing a specific photocurrent, it follows that the analysis of experimental data in terms of system parameters will require a sufficiently comprehensive data set that will allow differentiation between alternative interpretations. For instance: A low photocurrent may be the result of a low optical absorption coefficient at the given photon energy, but it may also be due to significant geminate recombination of the photo-generated electron-hole pairs, or reflect the formation of excitons. The combined use of different types of photoconductivity experiments is, therefore, often advisable, as is the combination of photoconductivity with related experiments such as photoluminescence or charge collection.

A wide variety of experimental techniques based on photoconductivity have come into use over the years. They can be divided into two main groups, one involving steady-state photoconductivity (SSPC) where the focus is on the stationary photocurrent levels, and a second one involving transient effects (TPC) where the time evolution of the photocurrents is being studied. We will use this division in our survey of the various methods, but should point out that SSPC can be measured through ac excitation. The information that can be obtained about the material under investigation is in general not specific for either the SSPC or TPC method that is used, but will depend on the wider context of the measurements. Recombination may be studied by means of TPC, but also the temperature dependence of SSPC can be used to identify different recombination mechanisms, while details of the electronic density of states (DOS) in the band gap of a semiconductor can be inferred either from the spectral response of SSPC or from a proper analysis of TPC. Detailed discussions of the general principles of photoconductivity may be found in the standard monographs by Bube [1, 2], Ryvkin [3] and Rose [4].

2. Steady-state photoconductivity methods

2.1. The basic single-beam experiment

The simplest photoconductivity experiment uses a constant monochromatic light source to generate equal excess densities of free electrons and holes, $\Delta n = \Delta p$, that lead to a change in the conductivity by

$$\Delta\sigma = \sigma_{\text{ph}} = e(\mu_n \Delta n + \mu_p \Delta p), \qquad (1)$$

where e is the electronic charge and μ_n, μ_p the electron, respectively hole mobility. The basic experimental arrangement is illustrated in Fig. 1(a), where L ands A are the length and cross-sectional area of the sample and the photocurrent I_{ph} corresponds to $\sigma_{\text{ph}} AF$, with $F = V/L$ being the applied electric field. The end surfaces of the sample are covered by a metallic electrode. However, since materials of present-day interest are often used in thin-film rather than bulk form, interdigitated electrodes of the type shown in Fig. 1(b) are frequently used as actual measurement geometry. In general, a fraction of the photogenerated carriers becomes immobilized by trapping at various defects such that not every part of Δn and Δp contributes equally to the photoconductivity in Equation 1. The effect of such trapping on the photoconductivity is reflected in the use of values for the mobilities μ_n andμ_p that are lower—and not necessarily symmetrically lower—than the theoretical free-carrier mobility μ_0. In fact, for a significant number of materials with widespread practical applications, either the $\mu_n \Delta n$ or the $\mu_p \Delta p$ product turns out to be much larger than the other one because of strongly unequal carrier mobilities. For instance, in intrinsic silicon the electron term dominates, while the photocurrent in chalcogenide glasses is carried by holes. In those instances, Equation 1 effectively reduces to a one-carrier equation.

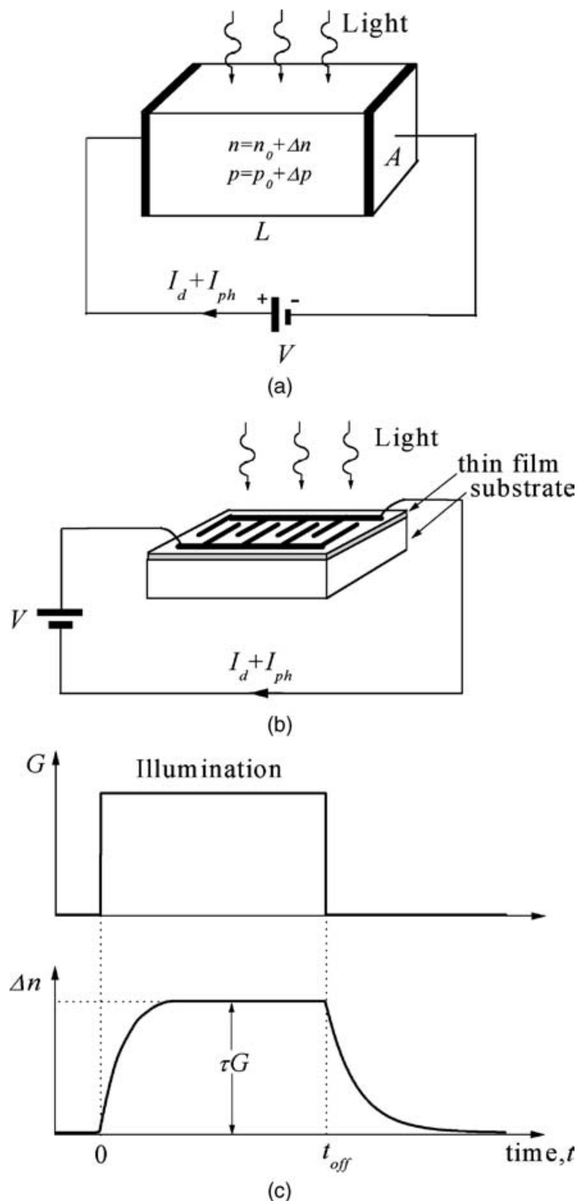

Figure 1 (a) Basic arrangement for photoconductivity measurements, with V the applied voltage and L, respectively A, the sample length and cross-sectional area. I_d, n_0 and p_0 are the current and the carrier densities in the dark, and I_{ph}, Δn, Δp are the incremental values caused by the illumination. (b) Example of interdigitated electrode configuration for a thin-film sample. (c) Schematic time development of the excess carrier concentration Δn in response to a period of illumination.

In the $\mu_n \Delta n$ or $\mu_p \Delta p$ product, the mobility μ_i is a material parameter that, in general, will depend on temperature and sample characteristics, while the excess carrier density $\Delta n = \Delta p$ is determined by a combination of material and external parameters. Phenomenologically, the excess density Δn can be written as a product $G\tau_i$, where G is the generation rate of free electrons and holes per unit volume and τ_i the average lifetime of the excess carriers. Introducing these quantities into Equation 1 leads to the form

$$\sigma_{\text{ph}} = eG(\mu_n \tau_n + \mu_p \tau_p), \qquad (2)$$

which explicitly displays the mobility-lifetime products that are frequently used as characterizing property of a photoconductor. The relationship between the steady-state values of Δn and G is illustrated in Fig. 1(c) where also the build-up and decay of Δn upon turn-on and turn-off of the illumination are shown. Those time-dependent aspects of photoconductivity will be addressed in a later section.

The generation rate G is defined by

$$G = \eta(I_0/h\nu)(1 - R)[1 - \exp(-\alpha d)]/d, \qquad (3)$$

where η is the quantum efficiency of the generation process, I_0 the incident illumination intensity (energy per unit time and unit area), $h\nu$ the photon energy, R the reflection coefficient of the sample, α the optical absorption coefficient of the material and d the sample thickness. A quantum efficiency $\eta < 1$ signifies that, as a result of geminate recombination of the carriers or of exciton formation, not every absorbed photon generates a free electron and hole that will contribute to the photocurrent. The values of the parameters η, R, and α depend, in general, on the wavelength of the illuminating light. Consequently, monochromatic illumination from a tunable light source can be used to obtain energy-resolved information about the sample, while white-light illumination will only offer a global average. Under many experimental circumstances the condition $\alpha d \ll 1$ will hold over a significant energy

range, i.e. the sample thickness is small with respect to the optical absorption depth of the material. Equation 3 can then be simplified to

$$G \cong \eta(I_0/h\nu)(1-R)\alpha. \quad (4)$$

The free-carrier lifetimes of the excess electrons and holes, τ_n and τ_p, of Equation 2 are governed by recombination with carriers of the opposite sign. Assuming, for simplicity, the frequently encountered case of photoconductivity dominated by one type of carrier (designated as majority carrier), and assuming the electron to be that majority carrier, the recombination rate can be written as $\tau_n^{-1} = b(p_0 + \Delta p)$ with b a recombination constant, and p_0 and Δp the equilibrium and excess minority carrier densities. It then follows that the photoconductivity

$$\sigma_{\text{ph}} \propto \Delta n = G\tau_n = G/b(p_0 + \Delta p) = G/b(p_0 + \Delta n). \quad (5)$$

Equation 5 indicates that a linear relationship $\sigma_{\text{ph}} \propto G$ holds for $\Delta n \ll p_0$, i.e. for low excess carrier density, while high excitation levels with $\Delta n \gg p_0$ lead to $\sigma_{\text{ph}} \propto G^{1/2}$. These linear and quadratic recombination regimes are also referred to as mono- and bimolecular recombination. For a given light source and temperature, variations in G correspond to variations in the light intensity I_0, and therefore $\sigma_{\text{ph}} \propto I_0^\gamma$ with $1/2 \leq \gamma \leq 1$. The value of γ itself will of course depend on the light intensity I_0. However, I_0 is not the only factor that determines the value of γ: Intermediate γ values may indicate a $\Delta n \approx p_0$ condition, but they may equally be caused by a distribution of recombination centers as outlined below [4].

For materials characterization, SSPC offers the possibility of using the above equations for determining the absorption coefficient in function of the energy of the incoming photons, and thus explore the electronic density of states around the band gap of a semiconductor. When single-crystalline samples of materials with sufficiently well-defined energy levels are studied, maxima corresponding to specific optical transitions may be seen in the photoconductivity spectra. A recent example, involving the split valence band of a p-$CdIn_2Te_4$ crystal, may be found in You *et al.* [5]. In disordered semiconductors with a significant distribution of localized states in the bandgap, photocurrents can be generated over a wide spectral range. Such is the case for the broad band seen in Fig. 2. This band relates to an amorphous $(Ge_2Se_7)_{88}Bi_5Sb_7$ bulk sample. The much sharper and more intense band that is also seen in Fig. 2 at 390 nm (3.2 eV) is due to Bi_2Se_3 crystallites that formed in the glass after annealing at 150 °C. Their subsequent room-temperature re-integration into the amorphous background could be followed over many months through the diminishing strength of the 390 nm line. A further example involving material defects is given in Fig. 3 where the photocurrent spectral distribution is shown for optical quality diamond films prepared by chemical vapor deposition [6]. The rise in photocurrent around 5.5 eV corresponds to the optical gap of diamond, while the shoulders at ~1.5 and ~3.5 eV signal the presence of defect distributions in the gap. The data in Fig. 3 were obtained under ac conditions by using chopped light and a lock-in amplifier. The changes in the observed phase shift can then also be used to locate the energies at which transitions to specific density of states (DOS) features become of importance. The use of ac excitation and lock-in detection has the added advantage of strongly reducing uncorrelated noise, but care must be taken that the ac frequency remains lower than the response rate of the investigated system over the spectral range of interest.

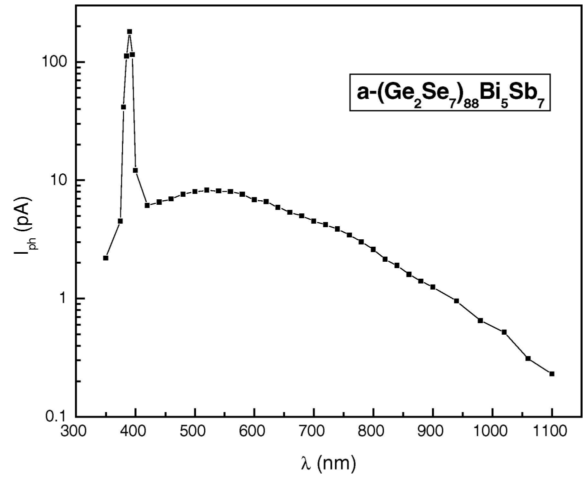

Figure 2 Spectral distribution of room-temperature photocurrent in a bulk amorphous $(Ge_2Se_7)_{88}Bi_5Sb_7$ gap cell after annealing at 150 °C during 15 hours (Adriaenssens, unpublished results).

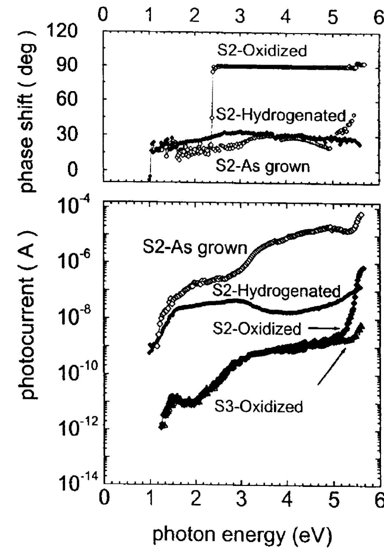

Figure 3 Room temperature ac photocurrent spectra, measured at 7 Hz, after various treatments of CVD diamond layers deposited at 920 °C (S2) and 820 °C (S3) (from Nesládek *et al.* [6]).

The equilibrium free-carrier densities n_0 and p_0, which play a role in the recombination process, depend on the temperature through the standard Fermi-Dirac occupation probability function $\exp[(E - E_F)/kT]$, thus making recombination a temperature-dependent process. In photoconductors, recombination is mediated by carrier traps in the band gap. The presence

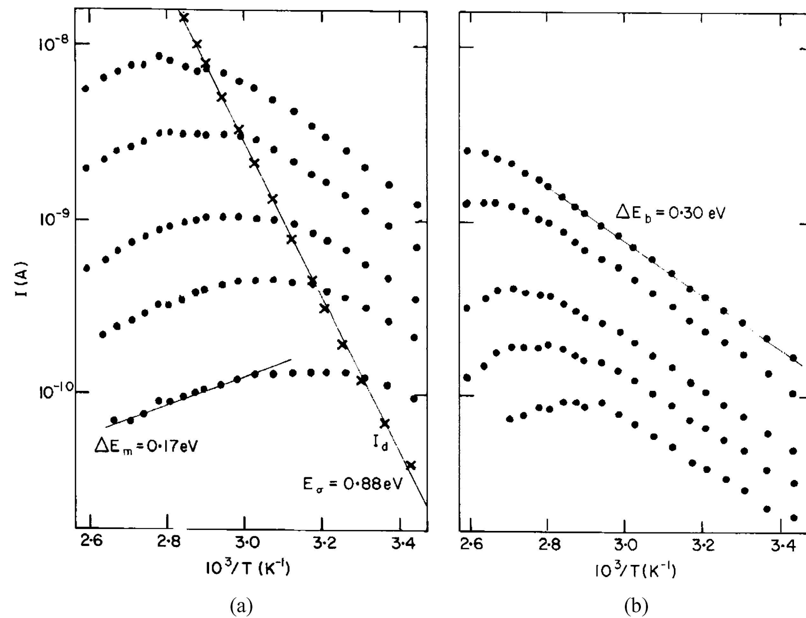

Figure 4 Temperature dependence of the steady-state dark and photocurrents in an a-As_2Se_3bulk sample, illuminated at 1.55 eV with intensities of 0.84, 3.5, 9.8, 38 and 120 × 10^{12} photons/cm^2.s (a), and illuminated at 1.85 eV with intensities of 0.56, 1.7, 4.6, 27 and 77 × 10^{12} photons/cm^2·s (b). ΔE_m and ΔE_b represent the photocurrent activation energies in the monomolecular and bimolecular recombination regimes respectively, and E_σ is the activation energy of the dark current I_d (from Adriaenssens [9]).

of discrete trapping levels leads to thermally activated photocurrents, with the activation energy indicating the energy position of the traps. Main and Owen [7] and Simmons and Taylor [8] showed that the positive photocurrent activation energy in the monomolecular recombination regime corresponds to the distance above the Fermi level of a donor-like center, while a negative activation energy value in the bimolecular region refers to the energy position above the valence band edge of an acceptor-like center. Fig. 4 illustrates this photocurrent behavior for amorphous As_2Se_3 [9]. The above pattern is characteristic for the group of chalcogenide glasses where the intrinsic charged defects with negative effective correlation energy act as recombination centers [10]. SSPC measurements can thus determine the recombination levels of those defects.

In highly photosensitive materials such as selenium or hydrogenated amorphous silicon (a-Si:H), measurements in the monomolecular region are hindered by the difficulty of satisfying the $\Delta n \ll p_0$ condition. In addition, the SSPC temperature dependence in a-Si:H does not exhibit a definite activation energy due to the presence of a more distributed and complex set of traps that even induce regions of superlinear dependence on light intensity [11]. It illustrates that SSPC analysis is not necessarily straightforward.

Whenever the electronic density of states in the band gap of a photoconductor consists of a distribution of traps (as is the case in amorphous materials), a quasi-Fermi level $E_{\mathrm{qF}} = E_F - kT\ln(1 + \Delta n/n)$, linked to the excess carrier density, can be defined. This quasi-Fermi level will—to first approximation—correspond to the demarcation level that divides the DOS into a shallower part where carriers will be trapped and subsequently re-emitted and a deeper part where traps have become recombination centers. In other words, varying light intensities influence both carrier generation as well as recombination rates. When several trapping centers with quite different characteristics are present in the photoconductor, shifts in the position of the quasi-Fermi levels can then produce unexpected results. Instances of $\sigma_{\mathrm{ph}} \propto I_0^\gamma$ with $\gamma > 1$ (as referred to above) will be observed for some materials, while combinations that actually produce *negative* photoconductivity, $\sigma_{\mathrm{ph}} < 0$, have also been encountered [4].

2.2. CPM: The constant photocurrent method

The constant photocurrent method (CPM) has been proposed by Vaněček and co-workers [12, 13] to determine the optical absorption coefficient as a function of photon energy, $\alpha(E)$, by means of Equations 2–4. In CPM, the photocurrent is kept constant by continuous adjustment of the light intensity I_0 while the photon energy is scanned across the spectrum. The constant photocurrent implies an immobile position of the quasi-Fermi levels and thus a constant free carrier lifetime τ. It then follows that in

$$\sigma_{\mathrm{ph}} = e\mu\tau(I_0/h\nu)(1 - R)\eta\alpha \quad (6)$$

the product $(I_0/h\nu)\alpha$ will remain constant, and that α can be determined from it, provided the energy dependence of the parameters μ, R and η of Equation 6 is negligible. The value at which the photocurrent is fixed can be freely chosen, but will in practice be dictated by the low-absorption region of the sample. However, since even low-level photocurrents can still be measured with high precision, the method is especially useful at low values of the optical absorption where standard transmission measurements lose their accuracy.

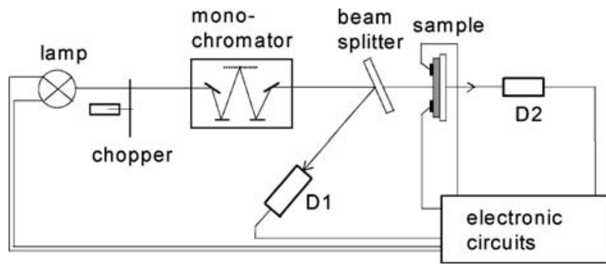

Figure 5 Schematic diagram of an 'absolute' CPM set-up. Photodetector D1 is used for measuring the intensity of the lamp, while detector D2 measures the transmitted light (after Vaněček *et al.* [13]).

In 'absolute' CPM, optical transmission through the film is measured simultaneously with the photocurrent and the data of the two measurements are combined to remove optical interference fringes from the data and fix the value of the proportionality constant [13]. The experimental arrangement used in such absolute CPM measurements is schematically shown in Fig. 5. The CPM experiment can be operated with either dc or ac illumination, but the retrieved absorption spectra will not be identical. AC illumination can be obtained by the use of a mechanical chopper (as suggested in Fig. 5), but also, for instance, from an ac-driven light-emitting diode. Main *et al.* [14] showed that, in the dc mode, transitions involving initially unoccupied DOS levels raise the absorption above the value that is seen with the ac technique. Systematic comparison of dc and ac results allows, therefore, to distinguish between occupied states below the operative Fermi level and unoccupied ones above it. In cases where the quantum efficiency of carrier generation, η, may be taken as unity, CPM gives $\alpha(E)$ directly as $1/I_0$ and the method is widely used, as has been the case for hydrogenated amorphous silicon. However, for materials such as chalcogenide glasses or organic semiconductors where η itself is energy-dependent, it is only the product $\eta\alpha$ that is readily obtained.

2.3. DBP: Dual beam photoconductivity

Like the CPM discussed above, the dual beam photoconductivity (DBP) technique is aimed at a determination of the sub-bandgap optical absorption in a photoconductor. A constant, uniformly absorbed illumination I_0 is used to establish a constant excess carrier density in the material, and hence a constant free-carrier lifetime τ. To this background, the chopped signal $I'(E)$ of a low-intensity, tunable light source is added to generate photoconductivity variations $\delta\sigma_{\mathrm{ph}}(E)$. Synchronous lock-in detection of the small ac signal then provides the needed information to deduce $\alpha(E)$. By carrying out measurements for differing values of the background illumination intensity, DBP allows the photoconductor absorption to be tested for changing positions of its quasi-Fermi levels. Changes in the resolved $\alpha(E)$ curves can then be used to obtain information on the DOS distribution in the sample. An example of such use of DBP may be found in Günes *et al.* [15] where differences in absorption between annealed and light-soaked hydrogenated amorphous silicon samples are studied.

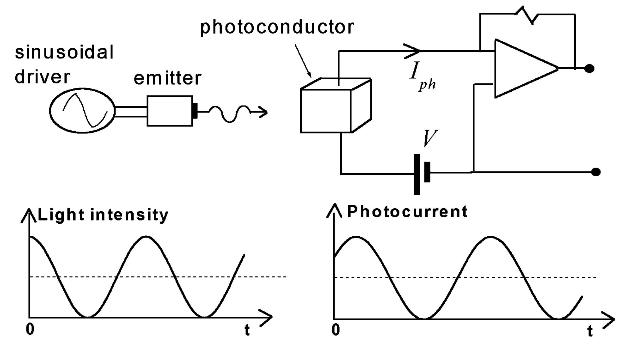

Figure 6 Schematic diagram of a MPC set-up (upper frames), and of the phase relationship between the exciting light intensity and the resulting photocurrent (lower frames).

2.4. MPC: Modulated photoconductivity

The experimental technique that has become known as Modulated Photoconductivity (MPC) seeks to determine the energetic distribution of states in the bandgap of a photoconductor from an analysis of the phase shift between an ac photo-excitation and the ensuing ac photocurrent in function of the modulation frequency of the light [16, 17]. Fig. 6 shows the essential parts of a MPC set-up, and illustrates the phase difference between the illumination and the photocurrent. Two modulation frequency ranges with distinct characteristics have been identified. In the high-frequency region, from a few Hz on into the kHz range, the signal is dominated by carrier release from traps with a release rate that matches the modulation frequency. The usual assumption that the release probability decreases exponentially with the trap depth according to $r \propto \exp(-E/kT)$ makes the link between the measured phase shift and the DOS of the material. The relationship between the two is expressed by

$$g(E) \propto \sin(\Phi)/I_{\mathrm{ac}}, \quad E = kT\ln(\nu_0/\omega) \tag{7}$$

where Φ and I_{ac} are the phase and intensity of the ac photocurrent, k is the Boltzmann constant, T the temperature, ν_0 the attempt-to-escape frequency and ω the modulation frequency. At the low-frequency end, recombination and trapping in deep states determine the phase shifts and the DOS varies according to $\tan(\Phi)/\omega$. The transition between the two regions is tied to the position of the quasi-Fermi levels and can, therefore, be shifted by changing the illumination intensity. MPC works best with photoconductors where one carrier type dominates the current, and therefore only one side of the bandgap need be taken into account in the analysis. An example of MPC-determined DOS profiles is given in Fig. 7 [18]. It shows the conduction-band side of the bandgap of a polymorphous silicon sample, as-deposited as well as following light soaking and after subsequent annealing.

3. Transient photoconductivity experiments

The study of transient aspects of photoconductivity can relate to either the build-up or relaxation of steady-state photocurrents, or to a material's response to pulsed

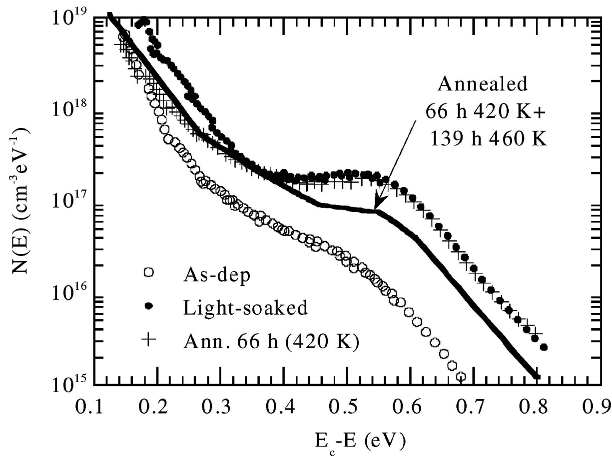

Figure 7 DOS below the CB edge of a polymorphous silicon sample deposited at 423 K, and measured by MPC as-deposited, after light soaking, and after two stages of subsequent annealing (from Longeaud *et al.* [18]).

excitation. While the SSPC turn-on transient reflects the interplay between generation and recombination of carriers—an interplay that often leads to a current overshoot at high excitation levels—, the SSPC relaxation upon turn-off only involves recombination and is therefore easier to analyse. Nevertheless, a simple exponential decay of the photocurrent as sketched in Fig. 1(c) will only be observed when a unique recombination path is followed, a situation that is the exception rather than the rule. Transient photoconductivity (TPC) caused by pulsed excitation is generally simpler to analyse. Indeed, whereas a quasi-equilibrium distribution of trapped photogenerated carriers will build up or be present in the photoconductor's bandgap under SSPC, the TPC experiments can be analysed against the background of the thermal equilibrium distribution of carriers in the material.

3.1. Current relaxation from the steady state

Upon termination of steady-state illumination, the generation term drops out of the rate equation that describes the non-equilibrium carrier distribution but the carrier density itself and the operative recombination process are not altered. Consequently, the initial photocurrent decay will be governed by whatever recombination mode existed under SSPC conditions. Spectroscopic analysis of the relaxation current in terms of the distribution of states in the bandgap can readily be achieved in the case of monomolecular recombination [19] with the product of photocurrent and time being proportional to the DOS:

$$I_{\text{ph}}(t) \cdot t \propto g(E), \quad E = kT \ln(\nu_0 t). \tag{8}$$

In Equation 8, kT is the Boltzmann energy and ν_0 is the attempt-to-escape frequency. When, on the other hand, bimolecular recombination dominates, the link between the current and the distribution of recombination centers is much less direct and spectroscopic analysis is difficult. Unfortunately, bimolecular recombination is dominant in good photoconductors.

In spite of the above, relaxation of the steady-state current has often been used to obtain a first-order estimate for free-carrier lifetimes, be it that this had to be done on a purely phenomenological basis due to the lack of sufficient information on the recombination mechanisms involved. An exponential fit to the initial part of the decay is then often used for making the estimate. In cases where more than one, sometimes vastly different recombination mechanisms are operative, this initial decay does not necessarily represent the most significant part of the carriers. Such is certainly the case whenever so-called persistent photoconductivity is observed; one of the relaxation times involved is then longer than the observation time.

3.2. TPC: Transient photoconductivity

In the standard transient photoconductivity (TPC) experiment, free carriers are excited into the transport band at time $t = 0$ by a short light pulse. They are then moved along by the electric field until their eventual disappearance through recombination, but before this happens they will have been immobilized a number of times by various traps that are present in the material. Since the carrier distributions are in thermal equilibrium at the start of the experiment, both the trapping sites for electrons above the Fermi level and the hole trapping sites below E_F are empty, such that the newly created carriers are not excluded from any of those trapping sites. Given that carrier release from a trap is a thermally activated process with the trap depth being the activation energy, deeper traps immobilize carriers for longer times and lead to lower values of the transient current. As shallower states release trapped carriers sooner, retrapping of those carriers will lead to an increasing occupation of the deeper states and further reduction of the current level. To allow this thermalisation of the excited carriers to run its full course until recombination sets in, the experiments are traditionally carried out in the so-called secondary photocurrent mode whereby the sample is supplied with ohmic electrical contacts and carrier loss is by recombination only. Co-planar electrode geometries (gap cells) are mostly used. Expressions that link the transient current to the distribution of localized states can be derived [20], but they are difficult to invert in the general case. Nevertheless, as long as recombination can be neglected, a relationship $g(E) \propto [I(t) \cdot t]^{-1}$ can be used as first-order estimate.

For the special case of an exponential DOS, the solution is straightforward: A $g(E) \propto \exp(-E/E_0)$ distribution of trapping levels leads to a power-law for the transient current $I(t) \propto t^{-(1-\alpha)}$ with $\alpha = kT/E_0$. In other words, the width of the exponential distribution, E_0, can be deduced from the slope of the power-law decay of the current. Essentially exponential distributions were found to dominate the valence band tail of equilibrated amorphous As_2Se_3 samples over a wide energy range [9], but no other examples have emerged.

An elegant way to circumvent the difficulties posed by a time-domain analysis of the transient current is to transpose the current decay into the frequency domain

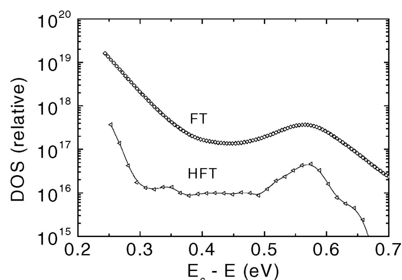

Figure 8 DOS below the conduction band edge in a-Si:H, obtained through Fourier transforms of the transient photocurrent; HFT: the high-resolution analysis of Main [22], FT: the earlier analysis according to Main *et al.* [21].

by Fourier transform [21]. Since the TPC current decay is the photoconductor's response to an impulse excitation, its Fourier transform gives the frequency response $I(\omega)$ of that photoconductor. In fact this $I(\omega)$ corresponds to the photocurrent intensity I_{ac} as used in the MPC method, and the same procedures can thus be used to extract the information on density and energy distribution of localized states in the band gap. Not just Fourier transform, but also Laplace transform techniques have been applied to the conversion of TPC signals into DOS information. A comparison and discussion of the results may be found in Main [22]. Examples of Fourier-transform TPC analysis as originally proposed and as developed since are shown in Fig. 8 for an a-Si:H sample. Whereas the energy range that can be probed is limited in MPC by the frequency range of the lock-in amplifier, it is the smallest resolution time of the detection system that limits the range in the case of TPC, the latter one being generally more advantageous.

3.3. TOF: Time-of-flight measurements

The time-of-flight (TOF) experiment, originally designed to determine the drift mobility of free carriers in high-mobility materials, has proved most successful in its adaptation for low-mobility materials such as organic or amorphous semiconductors [23]. There it has been used for drift mobility measurements but also as an alternative TPC technique to study the energy distribution of localized states. While majority carriers will dominate photocurrents in traditional TPC, TOF allows independent measurements with majority and minority carriers, and thus independent examinations of the valence-band side and conduction-band side of the band gap.

For TOF measurements, the sample consists of a layer of the photoconducting material sandwiched between two electrodes that are blocking for carrier injection into the sample. At least one of the electrodes has to be semi-transparent to permit the photo-excitation of free carriers in the material just beyond the illuminated contact by a strongly absorbed light flash. Depending on the polarity of the electric field applied across the sample, either electrons or holes will then be drifted through the sample. At their arrival at the back contact the current will drop since the blocking contact ensures that only the primary photocurrent is measured. From the transit time t_T, i.e. the time needed for the charge sheet to cross the sample, the drift mobility μ_d can be calculated according to $\mu_d = L/t_T F$, where L is the sample length and F the applied electric field. The essential elements of a TOF measuring circuit are displayed in Fig. 9. The transit time can be measured directly on the current trace, in which case it is variously defined as the time at which the current has dropped by values going from 10 to 50% (the latter one being most commonly used), or it can be obtained by integrating the current and using the time at which the collected charge saturates. Obtaining a true value of μ_d requires that the field F be uniform and constant during the carrier transit, which means that F should only be applied a short time before the optical excitation and that the transit time should be short with respect to the dielectric relaxation time in the material. Fig. 10 shows TOF transients in a conjugated polymer whereby a 10% drop is used as transit time definition.

In materials with a wide distribution of localized gap states, as is generally the case in disordered photoconductors, the drifting charge package spreads out along the length of the sample, and a representative transit time can only be discerned as a change of slope in

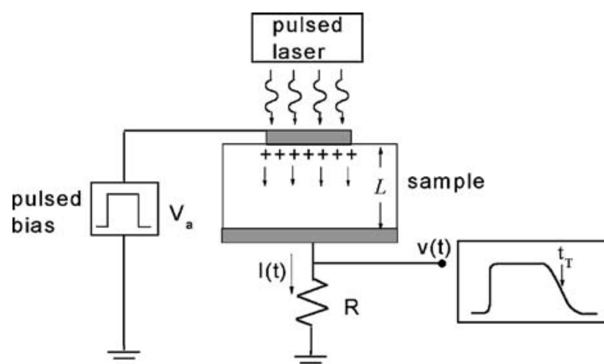

Figure 9 TOF measurement set-up shown for the case of holes being drifted through the length L of the sample by a positive applied voltage. The resistor R that generates an output voltage can be chosen low to minimize RC distortion of the signal at short times, or high to enhance detectability of weak signals at the expense of time resolution.

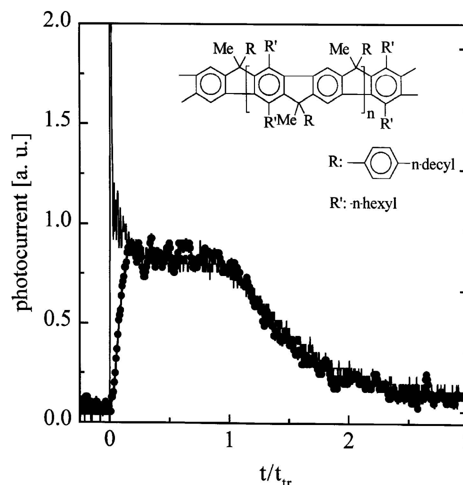

Figure 10 Time-of-flight transients measured at 243 K in Methyl-substituted ladder-type poly(para)phenelene (MeLPPP) with 60 kV/cm (line) and 300 kV/cm (●) applied, and normalized to a transit time set at 90% of the pre-transit current. The inset shows the chemical structure of MeLPPP (from Hertel *et al.* [24]).

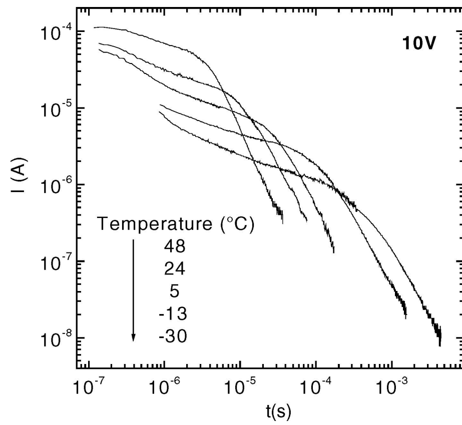

Figure 11 Example of TOF hole transients measured at several temperatures as indicated, with 10 V applied across a 5.6 μm thick a-Si:H sample grown in an expanding thermal plasma at 0.85 nm/s and 250 °C substrate temperature, and sandwiched between Mo contacts (from Brinza *et al.* [25]).

a double-logarithmic plot of current versus time. The curves in Fig. 11 [25] illustrate such behavior. Measurements at different temperatures and applied fields are then needed to ascertain that the observed feature marks an actual carrier transit rather than deep trapping of the photogenerated charge. In the materials that exhibit this anomalously dispersive transport, the pre-transit current will have the characteristics of the TPC described in the previous section and the information about the distribution of gap states $g(E)$ that is contained in the current transient can be extracted in the same ways. Not just the pre-transit current transients but also the measured drift mobility values have been employed in the past to estimate the DOS in the band tails of disordered semiconductors. In the latter case, specific $g(E)$ functions are explored through trap-controlled transport modelling to reproduce the experimental dependence of μ_d on temperature and electric field. This technique has since been replaced by the more direct procedures described in preceding sections.

At times longer than the TOF transit time, a steeper current decay testifies to the fact that carriers are leaving the sample. The post-transit current that is then observed is increasingly due to the emission of carriers that were trapped in states deep in the bandgap. Provided that the conditions are such that the probability of subsequent deep retrapping of the same carriers is negligible, a proper analysis of these post-transit TOF current transients permits the elucidation of the distribution of localized states deeper in the gap [26] with, as in Equation 8, $g(E) \propto I(t) \cdot t$ expressing the correspondence. An example of such post-transit analysis of the DOS on the valence band side of a hydrogenated amorphous silicon sample is shown in Fig. 12. The resolved energy range, $E = kT \ln(\nu t)$, does shift with changes in the measurement temperature T.

3.4. IFTOF: Interrupted field time-of-flight

The interrupted field time-of-flight (IFTOF) experiment differs from the time-of-flight experiment described in the previous section in that the applied field that drives the photogenerated carrier packet through the sample is turned off for some period of time before the carriers have completed their transit. As illustrated in Fig. 13, when the field is turned on again a lower current intensity is measured, signalling that part of the drifting carriers have become immobilized in deep traps [29]. By studying the current drop as a function of the interruption time t_i, the deep-trapping lifetime of the carriers can be evaluated. Recombination can routinely be neglected in TOF experiments since only one type of carrier drifts through the sample, but by charging a sample with carriers of one polarity before performing an IFTOF experiment that drifts carriers of the opposite polarity through the sample, recombination parameters can be studied as well [30].

Another interesting method for studying the recombination process is—just like IFTOF—based on a simple modification of the TOF experiment: After generating free carriers through one contact and drifting the slower type of carrier into the sample, a second light pulse through the other contact sends a sheet of the oppositely charged carriers towards the first one. The two carrier packages will cross and some electrons and holes will recombine during that crossing, thereby affecting the observed current levels and opening a way to study the recombination process. A nicely worked-out example of the application of this technique with amor-

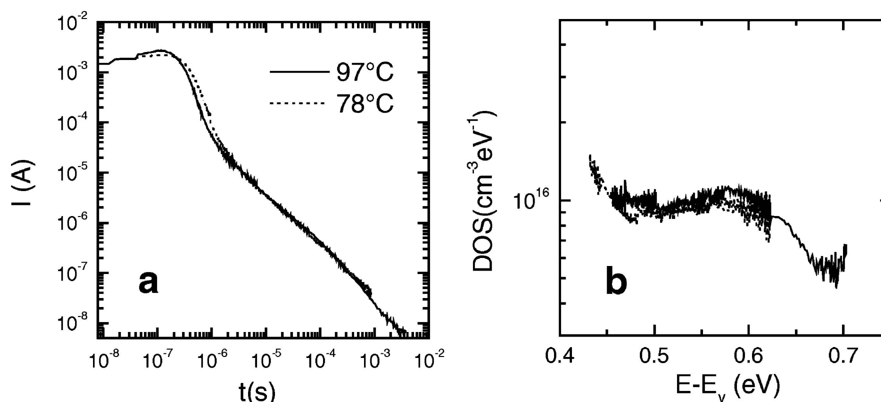

Figure 12 (a) TOF hole transients, showing the post-transit regime, from a 2 μm thick a-Si:H sample deposited at 6 nm/s and 450 °C, and with 10 V applied; (b) DOS profile calculated from them with Equation 2, $Q_0 = 2 \times 10^{-9}$ C, $\nu = 10^{12}$ s^{-1}, $g(0) = 10^{21}$ cm^{-3} eV^{-1} and $\mu_0 = 8$ cm^2 V^{-1} s^{-1} (from Brinza and Adriaenssens [27]).

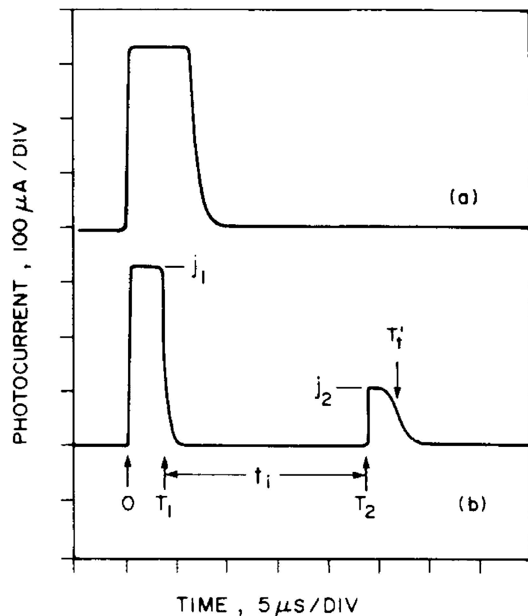

Figure 13 Comparison of current traces in TOF (a) and IFTOF (b) experiments. The applied electric field is turned off in case (b) for the length of time t_i (from Kasap *et al.* [28]).

phous selenium, may be found in Haugen and Kasap [31].

4. Related topics

The optical excitation of charge carriers that constitutes the essential initial condition for all photoconductivity phenomena, also leads to a number of other related materials characterisation techniques. Some are complementary in nature, but some of them do, in fact, differ from photoconductivity in name only.

4.1. PL: Photoluminescence

Photoluminescence (PL) and photoconductivity are complementary as well as competing processes. Luminescence is observed when photo-excited carriers do recombine radiatively, which obviously removes them from the carrier density that can contribute to the photoconductivity. The radiative recombination will mostly occur at specific lattice defects and can thus serve to characterize those defects. Coupling of the defect to the lattice will further introduce vibronic sidebands next to the PL line. They mark transitions that are shifted down (Stokes lines) or up (anti-Stokes) in energy from the main PL transition by the energy of one or more lattice phonons. Like the SSPC spectral distribution is related to the optical absorption spectrum of a substance (Section 2.1), there is a link between PL and the photoluminescence excitation (PLE) spectrum that characterizes the absorption at the luminescing centres. Such PLE spectrum also shows the vibronic structure, as illustrated for chemical-vapour-deposited diamond in [32]. While these vibronic lines can—in principle—also be observed in a SSPC spectrum, they are less well resolved there due to the dispersion that is inherently part of the electronic transport process. A general introduction to the subject of luminescence may be found in [33].

4.2. TRMC: Time-resolved microwave conductivity

Since the conductivity of a sample will determine to what extent incoming microwave power is reflected, measuring the changes in sample reflectivity upon illumination will indicate the conductivity changes, i.e. the photoconductivity. An advantage of this technique is that it does not require the deposition of electrodes on the material to be studied. Kunst and Werner [34] showed that identical photocurrent transients could be measured in a-Si:H by either TRMC or by the traditional TPC technique.

4.3. IPE: Internal photoemission

Whereas photoemission spectroscopy is based on the study of the energy spectrum of electrons that are emitted from a substance after excitation by, for instance, X-ray photons, in the case of internal photoemission (IPE) spectroscopy the photo-excited electrons never leave the sample and they are detected by means of a photocurrent measurement. However, the sample is now in general an interface between two different materials [35], rather than simply a homogeneous material to be characterized. In other words, the emission refers to the electron transfer from one substance into the other one. Examples of IPE spectral curves, measured by Afanas'ev *et al.* [36] on barriers between thin layers of SiO_2, Al_2O_3, ZrO_2 or combinations thereof, and (100)Si, are presented in Fig. 14. They show the energy dependence of the IPE yield, defined as the photocurrent normalized to the incident photon flux, from which the energy barriers Φ at the interfaces can be determined.

4.4. Spin-dependent recombination

Recombination, whether it happens non-radiatively or radiatively, plays a crucial role in both PL and PC. However, for recombination to be possible the electron and hole involved must have opposite spins, i.e. they must form a singlet spin state. Recombination is not possible for carriers linked in the more probable triplet state, but it can be enabled by flipping one of the spins by spin resonance [37]. The combination of photoconductivity and spin-dependent recombination has been developed as a sensitive detection technique for electron spin resonance (ESR) in disordered semiconductors [38]. In the ESR experiment, an applied magnetic field will split the spin Zeeman levels and a resonant microwave field will equalize the singlet and triplet populations, thus enhancing the recombination probability of any non-equilibrium carrier density. Consequently, the photoconductivity of the system under investigation will drop when the resonance condition is achieved. In a-Si:H this way of detecting the spin resonance proved to be much more sensitive than the traditional measurement of the absorbed power [37, 38].

4.5. PICTS: Photo-induced current transient spectroscopy

The photo-induced current transient spectroscopy (PICTS) is often used for the investigation of discrete

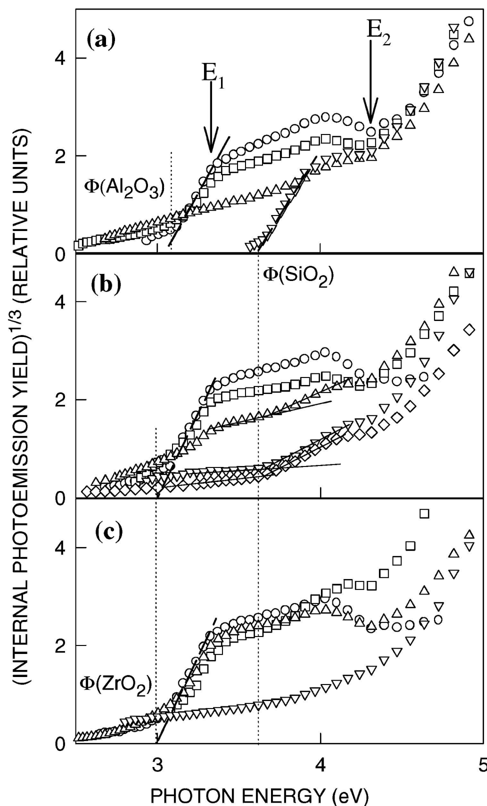

Figure 14 Energy dependence of IPE yield across insulator/(100)Si interfaces, the insulator being (a) 5-nm-thick Al_2O_3 (○) or the same Al_2O_3 stacked with either 1.2 nm (□) or 2.5 nm (△) SiO_2, all compared to a single 4.1 nm SiO_2 layer (∇); (b) 7.4 nm ZrO_2 (○), and stacks of 0.5 nm SiO_2/5 nm ZrO_2 (□), 1.3 nm SiO_2/5 nm ZrO_2 (△), 2.5 nm SiO_2/7.4 nm ZrO_2 (∇), 3.2 nm SiO_2/7.4 nm ZrO_2 (◊); (c)7.4 nm ZrO_2 (○), stacks of 0.5 nm Al_2O_3/5 nm ZrO_2 (□), 1.5 nm Al_2O_3/5 nm ZrO_2 (△), and the latter after 10 min oxidation in O_2at 800 °C (∇). E_1 and E_2 indicate the onset of direct optical transitions in Si, and Φ shows the spectral thresholds due to the interface barriers. (From Afanas'ev *et al.* [36])

trapping levels in crystalline semiconductors and insulators [39]. The technique is similar to the relaxation from the steady state described in Section 3.1, but uses the change with temperature of the relaxation current difference at two fixed times in the current decay to locate the traps. An example of PICTS signals is shown

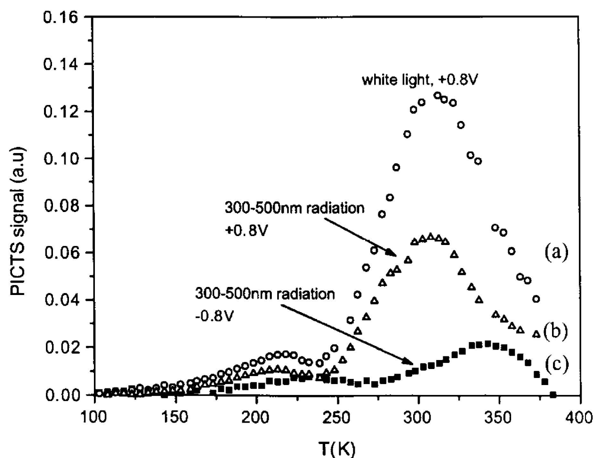

Figure 15 PICTS signals from a Au/CdTe cell, illustrating how electron (c) and hole traps (b) can be identified separately through the use of shallowly absorbed light and reversal of the applied voltage polarity. This distinction is lost when more uniform illumination of the cell is used (curve a). (From Mathew [40])

in Fig. 15. It illustrates how, with the use of shallowly absorbed light and depending on the polarity of the applied field, either electrons or holes will be preferentially trapped in the material. Electron and hole traps can thus be clearly identified.

Acknowledgment

The authors are grateful to the *Fonds voor Wetenschappelijk Onderzoek—Vlaanderen* for its financial support of their research through grant G.0381.01.

References

1. R. H. BUBE, "Photoconductivity of Solids" (Wiley & Sons, New York, 1960).
2. R. H. BUBE, "Photoelectronic Properties of Semiconductors" (Cambridge University Press, Cambridge, 1992).
3. S. M. RYVKIN, "Photoelectric Effects in Semiconductors" (Consultants Bureau, New York, 1964).
4. A. ROSE, "Concepts in Photoconductivity and Allied Problems" (Krieger, Huntington, 1978).
5. S. H. YOU, K. J. HONG, T. S. JEONG, C. J. YOUN, J. S. PARK, D. C. SHIN and J. D. MOON, *J. Appl. Phys.* **95** (2004) 4042.
6. M. NESLADEK, L. M. STALS, A. STESMANS, K. IAKOUBOVSKII, G. J. ADRIAENSSENS, J. ROSA and M. VANECEK, *Appl. Phys. Lett.* **72** (1998) 3306.
7. C. MAIN AND A. E. OWEN in "Electronic and Structural Properties of Amorphous Semiconductors", edited by P.G. Le Comber and J. Mort (Academic Press, London, 1973) p. 527.
8. J. G. SIMMONS and G. W. TAYLOR, *J. Phys. C : Solid State Phys.* **7** (1974) 3051.
9. G. J. ADRIAENSSENS, *Philos. Mag. B* **62** (1991) 79 and references therein.
10. G. J. ADRIAENSSENS and N. QAMHIEH, *J. Mater. Sci.: Mater. Electron.* **14** (2003) 605.
11. H. FRITZSCHE, B.-G. YOON, D.-Z. CHI, and M. Q. TRAN, *J. Non-Cryst. Solids* **141** (1992) 123.
12. M. VANECEK, J. KOCKA, J. STUCHLIK and A. TRISKA, *Solid State Commun.* **39** (1981) 1199.
13. M. VANECEK, J. KOCKA, A. PORUBA and A. FEJFAR, *J. Appl. Phys.* **78** (1995) 6203.
14. C. MAIN, S. REYNOLDS, I. ZRINSCAK and A. MERAZGA, *Mat. Res. Soc. Symp. Proc.* **808** (2004) 103.
15. M. GUNES, C. WRONSKI and T. J. MCMAHON, *J. Appl. Phys.* **76** (1994) 2260.
16. H. OHEDA, *ibid* **52** (1981) 6693.
17. R. BRUGGEMAN, C. MAIN, J. BERKIN and S. REYNOLDS, *Philos. Mag. B* **62** (1990) 29.
18. C. LONGEAUD, D. ROY and O. SAADANE, *Phys. Rev. B* **65** (2002) 85206.
19. M. S. IOVU, I. A. VASILIEV, E. P. COLOMEICO, E. V. EMELIANOVA, V. I. ARKHIPOV and G. J. ADRIAENSSENS, *J. Phys.: Condens. Matter* **16** (2004) 2949.
20. A. I. RUDENKO and V. I. ARKHIPOV, *Philos. Mag. B* **45** (1982) 209.
21. C. MAIN, R. BRUGGEMAN, D. P. WEBB and S. REYNOLDS, *Solid State Commun.* **83** (1992) 401.
22. C. MAIN, *J. Non-Cryst. Solids* **299** (2002) 525.
23. W. E. SPEAR, *ibid.* **1** (1969) 197.
24. D. HERTEL, A. OCHSE, V. I. ARKHIPOV and H. BAESSLER, *J. Imaging Sci. Technol,* **43** (1999) 220.
25. M. BRINZA, E. V. EMELIANOVA and G. J. ADRIAENSSENS, *Phys. Rev. B* **71** (2005) 115209.
26. G. F. SEYNHAEVE, R. P. BARCLAY, G. J. ADRIAENSSENS and J. M. MARSHALL, *ibid.* **39** (1989) 10196.
27. M. BRINZA and G. J. ADRIAENSSENS, *J. Optoelectron. Adv. Mater.* **7** (2005) 73.
28. S. KASAP, B. POLISHUK, D. DODDS and S. YANNACOPOULOS, *J. Non-Cryst. Solids* **114** (1989) 106.

29. S. KASAP, B. POLISHUK and D. DODDS, *Rev. Sci. Instrum.* **61** (1990) 2080.
30. S. KASAP, B. FOGAL, M. Z. KABIR, R. E. JOHANSON and S. K. O'LEARY, *Appl. Phys. Lett.* **84** (2004) 1991.
31. C. HAUGEN and S. O. KASAP, *Philos. Mag. B* **71** (1995) 91.
32. K. IAKOUBOVSKII and G. J. ADRIAENSSENS, *Phys. Rev. B* **61** (2000) 10174.
33. H. B. BEBB and E. W. WILLIAMS, in "Semiconductors and Semimetals" vol. 8, edited by: R. K. Willardson and A. C. Beer (Academic Press, New York, 1972) p. 181.
34. M. KUNST and A. WERNER, *J. Appl. Phys.* **58** (1985) 2236.
35. V. K. ADAMCHUK and V. V. AFANAS'EV, *Progr. Surf. Sci.* **41** (1992) 211.
36. V. V. AFANAS'EV, M. HOUSSA, A. STESMANS and M. M. HEYNS, *Appl. Phys. Lett.* **78** (2001) 3073.
37. M. STUTZMANN, M.S. BRANDT and M.W. BAYERL, *J. Non-Cryst. Solids* **266** (2000) 1.
38. K. LIPS, C. LERNER and W. FUHS, *ibid.* **198** (1996) 267.
39. P. BLOOD and J. W. ORTON, in "The Electrical Characterisation of Semiconductors:Majority Carriers and Electron States", edited by N. H. March (Academic Press, New York, 1992) p. 478.
40. X. MATHEW, *Sol. Energy Mater. Sol. Cells* **76** (2003) 225.

Received 11 May
and accepted 16 May 2005